

Electronic structures of quasi-one-dimensional cuprate superconductors $\text{Ba}_2\text{CuO}_{3+\delta}$

Kai Liu^{1,*}, Zhong-Yi Lu^{1,†} and Tao Xiang^{2,3‡}

¹*Department of Physics and Beijing Key Laboratory of Opto-electronic Functional Materials & Micro-nano Devices, Renmin University of China, Beijing 100872, China*

²*Institute of Physics, Chinese Academy of Sciences, Beijing 100190, China and*

³*Collaborative Innovation Center of Quantum Matter, Beijing 100190, China*

(Dated: February 1, 2019)

An intact CuO_2 plane is widely believed to be a prerequisite for the high- T_c superconductivity in cuprate superconductors. However, an exception may exist in the superconducting $\text{Ba}_2\text{CuO}_{3+\delta}$ materials where CuO chains play a more important role. From first-principles density functional theory calculations, we have studied the electronic and magnetic structures of $\text{Ba}_2\text{CuO}_{3+\delta}$. The stoichiometric Ba_2CuO_3 and Ba_2CuO_4 contain quasi-one-dimensional CuO chains and intact two-dimensional CuO_2 planes, respectively. In comparison with the nonmagnetic metal Ba_2CuO_4 , Ba_2CuO_3 is found to be an antiferromagnetic (AFM) Mott insulator. It possesses a nearest-neighbor intra-chain antiferromagnetic (AFM) coupling and a weak inter-chain interaction, and its lowest unoccupied band and highest occupied band are contributed by $\text{Cu } 3d_{x^2-y^2}$ -orbital (or $d_{x^2-y^2}$ -orbital if we denote the bc -plane as the xy -plane) and $\text{O } 2p$ -orbitals, respectively. Total energy calculations indicate that the oxygen vacancies in $\text{Ba}_2\text{CuO}_{3+\delta}$ prefer to reside in the planar sites rather than the apical oxygens in the CuO chains, in agreement with the experimental observation. Furthermore, we find that the magnetic frustrations or spin fluctuations can be effectively induced by moderate charge doping. This suggests that the superconducting pairing in oxygen-enriched $\text{Ba}_2\text{CuO}_{3+\delta}$ or oxygen-deficient $\text{Ba}_2\text{CuO}_{4-\delta}$ is likely to be mainly driven by the AFM fluctuations within CuO chains.

I. INTRODUCTION

The interplay between superconductivity and dimensionality is an interesting issue in condensed matter physics. In the well-known cuprate superconductors^{1,2}, whose superconducting transition temperature is highest at ambient pressure^{3,4}, a common feature is that they all contain quasi-two-dimensional CuO_2 planes^{5,6} from which the superconducting pairing emerges while other layers just serve as a charge reservoir. Similarly, superconducting condensation is also believed to take place predominately in quasi-two-dimensional FeX ($X=\text{As, Se, ...}$) layers in iron-based superconductors⁷⁻¹¹. In recent years, superconducting transitions have also been discovered in Bechgaard-salts organic superconductors^{12,13}, molybdenum chalcogenides^{14,15} and pnictides¹⁶, chromium pnictides¹⁷⁻²², bismuth iodide²³, nickel-bismuth compounds²⁴, and other quasi-one-dimensional materials.

More recently, high temperature superconductor $\text{Ba}_2\text{CuO}_{4-\delta}/\text{Ba}_2\text{CuO}_{3+\delta}$ has been successfully synthesized under high pressure by Jin and coworkers²⁵. There are two possibilities regarding the parent compound of these superconductors. One possibility is that Ba_2CuO_4 is the parent compound. High- T_c superconductivity emerges in $\text{Ba}_2\text{CuO}_{4-\delta}$ when some oxygens are removed from Ba_2CuO_4 . Another possibility is that Ba_2CuO_3 is the parent compound and the superconductivity emerges in $\text{Ba}_2\text{CuO}_{3+\delta}$ when more oxygens are doped to it. For the latter, unlike the parent compound of other cuprate superconductors, Ba_2CuO_3 does not contain CuO_2 planes. Instead, it contains only CuO chains and the copper-oxygen bond is compressed along the c -axis but stretched along the b -axis (the CuO chain direction).

In order to determine the pairing mechanism of electrons, it is crucial to know where the oxygen vacancies reside in the superconducting $\text{Ba}_2\text{CuO}_{4-\delta}/\text{Ba}_2\text{CuO}_{3+\delta}$ compounds. If the oxygen vacancies mainly occupy the apical sites, the CuO_2 planes remain intact as the other cuprate superconductors. Experimental measurements of neutron powder diffraction²⁶ and electron diffraction²⁷ for similar compounds, however, suggested that the oxygen vacancies reside mainly on the CuO_2 planes and the apical sites are fully occupied by oxygen atoms. In this case, there are no perfect CuO_2 planes. This implies that intact CuO_2 planes are not absolutely necessary in achieving high- T_c superconductivity.

In this paper, we address the above questions by calculating the electronic and magnetic structures of $\text{Ba}_2\text{CuO}_{3+\delta}$ using first-principles density functional theory. Our study shows that the parent compound is Ba_2CuO_3 , which is an AFM Mott insulator. In Sec. II, we first describe the method, and then discuss the numerical results for both stoichiometric $\text{Ba}_2\text{CuO}_3/\text{Ba}_2\text{CuO}_4$ and oxygen doped materials. A summary is given in Sec. III.

II. RESULTS

We performed the first-principles density functional theory calculations on the electronic and magnetic structures of undoped or doped Ba_2CuO_3 or Ba_2CuO_4 materials using the projector augmented wave (PAW) method²⁸ with the Vienna *ab initio* simulation package^{29,30}. The generalized gradient approximation (GGA) of Perdew-Burke-Ernzerhof (PBE) type was used in the construction of the exchange-correlation functional³¹. The plane-

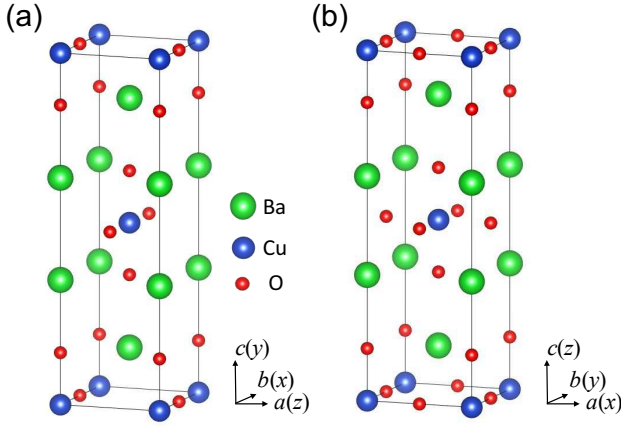


FIG. 1: Crystal structures of (a) Ba_2CuO_3 with CuO chains and (b) Ba_2CuO_4 with CuO_2 planes. Note the xy planes of Ba_2CuO_3 and Ba_2CuO_4 are defined differently in order to facilitate the discussion on orbitals.

wave basis set with a kinetic energy cutoff of 520 eV and a $12 \times 12 \times 4$ k -point mesh for the Brillouin zone sampling of conventional cell were adopted. The Fermi level was broadened by the Gaussian smearing method with a width of 0.05 eV. $\text{Ba}_2\text{CuO}_{3+\delta}$ can be regarded as a compound either by adding oxygen to Ba_2CuO_3 or by removing oxygen from Ba_2CuO_4 . Various locations of oxygen vacancies in $\text{Ba}_2\text{CuO}_{3+\delta}$ (or $\text{Ba}_2\text{CuO}_{4-\delta}$) were investigated with both the virtual crystal approximation (VCA) and the supercell methods. In the latter case, a $2 \times 2 \times 1$ supercell with different oxygen vacancy distributions was explored, while the lattice constants were fixed to the experimental values, and all internal atomic positions were allowed to relax until the forces on all atoms were smaller than 0.01 eV/Å. The correlation effect among Cu 3d electrons was incorporated using the GGA+U formalism of Dudarev *et al.*³² with a typical effective Hubbard interaction U of 6.5 eV.

A. Electronic and magnetic structures of stoichiometric Ba_2CuO_3 and Ba_2CuO_4

Figures 1(a) and 1(b) show the crystal structures of Ba_2CuO_3 and Ba_2CuO_4 , respectively. The former is composed of CuO chains along the b -axis, while the latter contains CuO_2 planes. In either case, Cu-O layers are separated by Ba-O layers. Cu atoms in both Ba_2CuO_3 and Ba_2CuO_4 form a square-like lattice in each ab -plane. Ba_2CuO_4 has the same lattice structure as La_2CuO_4 . However, it is only in Ba_2CuO_3 that Cu ions have the same nominal valence +2 as in La_2CuO_4 .

The a and b axes in Ba_2CuO_4 are equivalent because there are no O vacancies in the CuO_2 planes. However, they are not equivalent in Ba_2CuO_3 [Fig. 1(a)]. To determine the ground states of Ba_2CuO_3 and Ba_2CuO_4 , we calculated the energies of several representative magnetic states formed by Cu^{2+} ions and compared with that of

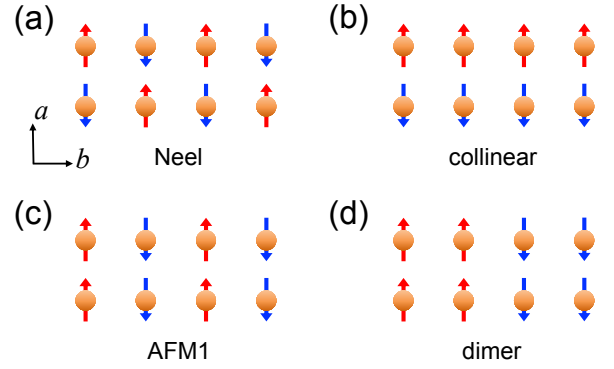


FIG. 2: Spin configurations of (a) AFM Néel state, (b) collinear AFM state, (c) AFM1 state, and (d) AFM dimer state for the Cu^{2+} spins in the ab plane. The brown balls denote Cu atoms. The red and blue arrows represent the up and down spins, respectively.

the nonmagnetic state. These magnetic ordered states, as partially shown in Fig. 2, include the standard AFM Néel state, the collinear AFM (or stripe) state, the AFM1 state in which Cu spins are antiferromagnetically coupled along the b -axis but ferromagnetically coupled along the a -axis, the AFM dimer state^{33,34} along the b -axis which is ferromagnetically coupled along the a -axis, and the ferromagnetic (FM) state.

For Ba_2CuO_3 , the relative energies of the above magnetic states with respect to the nonmagnetic state are given in Table I. All these magnetic states have lower energies than the nonmagnetic one. Among them, the AFM Néel state is energetically degenerate with the AFM1 state, and the collinear AFM state is energetically degenerate with the FM state. The ground state is found to have either the AFM Néel or the AFM1 order, indicating that there is a strong intra-chain AFM coupling along the b -axis but a weak inter-chain coupling along the a -axis. The AFM dimer state is next to the ground state in energy. In contrast, for Ba_2CuO_4 , all the above magnetic states are unstable and the ground state is nonmagnetic. From the calculations, we find that the weak inter-chain coupling in Ba_2CuO_3 is about 0.2 meV, smaller than the corresponding values in Ca_2CuO_3 (3.6 meV) and in Sr_2CuO_3 (0.8 meV)^{35,36}.

Figure 3 shows the total density of states (DOS) for Ba_2CuO_3 in the AFM Néel state and Ba_2CuO_4 in the nonmagnetic state, respectively. In contrast to Ba_2CuO_3 which is an AFM insulator, Ba_2CuO_4 is found to be

TABLE I: Relative energies (in unit of meV/Cu) of several magnetic states with respect to the nonmagnetic (NM) state for undoped Ba_2CuO_3 .

	Néel	collinear	AFM1	dimer	FM
Ba_2CuO_3	-180	-22	-180	-116	-22

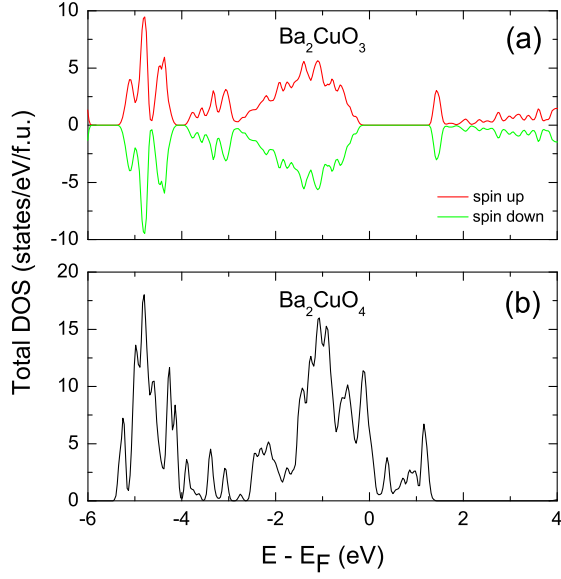


FIG. 3: Density of states (DOS) for (a) the AFM Néel state of Ba_2CuO_3 and (b) the nonmagnetic state of Ba_2CuO_4 .

a nonmagnetic metal. The calculated band gap of Ba_2CuO_3 is 1.2 eV, close to the experimental results for Ca_2CuO_3 (1.7 eV) and Sr_2CuO_3 (1.5 eV)³⁷. It should be pointed out that the AFM insulating ground state of Ba_2CuO_3 is obtained only when the on-site Hubbard interaction is included in the calculation. Without this interaction, the ground state is metallic. This suggests that Ba_2CuO_3 is an AFM Mott insulator³⁸, similar to La_2CuO_4 ³⁹.

We also calculated the partial density of states (PDOS) for Ba_2CuO_3 in the AFM Néel state (Fig. 4). For convenience, here we denote the b and c axes as the x and y axes [Fig. 1(a)]. Due to the nominal valence +2 of Cu ions in Ba_2CuO_3 , nine electrons fill the $3d$ orbitals of Cu atom. Among these $3d$ orbitals, the spin-minority $d_{x^2-y^2}$ orbital is mostly unoccupied [Fig. 4(a)]. The occupied bands are mainly contributed by O $2p$ orbitals. This results from the crystal field effect created by four O atoms surrounding a Cu atom in the bc plane. The PDOS peaks of unoccupied Cu $d_{x^2-y^2}$ and O $2p_x$ states appear at almost the same energy above the band gap. This indicates that there is a strong p - d hybridization between these orbitals.

Figures 5(a) and 5(b) show the calculated band structures of Ba_2CuO_3 along high-symmetry paths of the Brillouin zone in the nonmagnetic and the AFM Néel states, respectively. In the AFM state, the valence band maximum is located at the M point. Since the CuO chain is along b axis and the inter-chain couplings are rather weak, the band dispersions along the k_b direction are much larger than those along the other two directions.

In oxygen-enriched $\text{Ba}_2\text{CuO}_{3+\delta}$, the extra oxygens doped to Ba_2CuO_3 introduce hole doping, which is equivalent to shifting the Fermi energy down to the valence

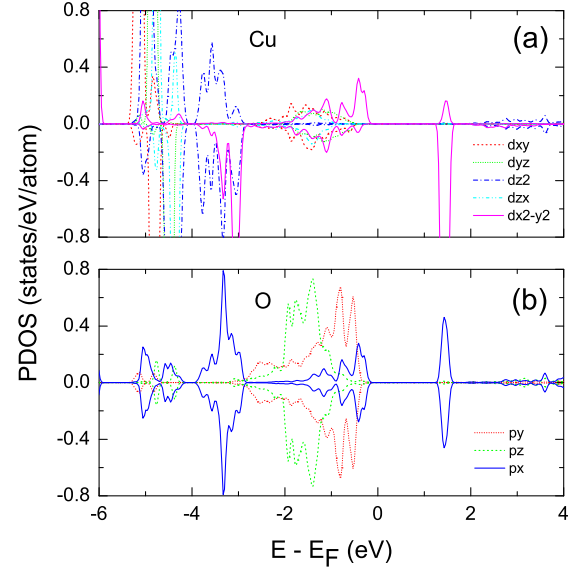


FIG. 4: Partial density of states (PDOS) for the AFM Néel state of Ba_2CuO_3 projected on (a) the $3d$ orbitals of Cu atom and (b) the $2p$ orbitals of O atom along the CuO chain. The up and down parts in each panel represent the spin-up and spin-down channels, respectively. The xy plane is defined in Fig. 1(a).

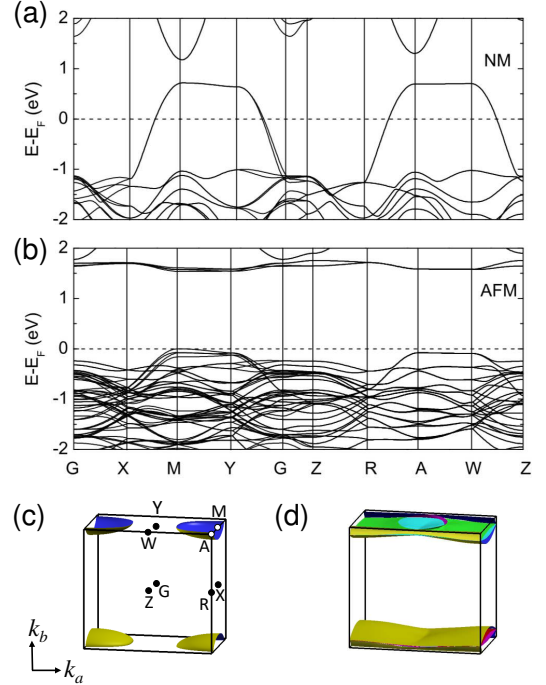


FIG. 5: Band structures of BaCuO_3 in (a) the nonmagnetic state with a conventional cell and (b) the AFM Néel state with a $2 \times 2 \times 1$ supercell. (c) and (d) show the Fermi surface contours in the AFM Néel state upon hole doping by rigidly shifting the Fermi level 0.05 eV and 0.1 eV below the top of the valence bands, respectively.

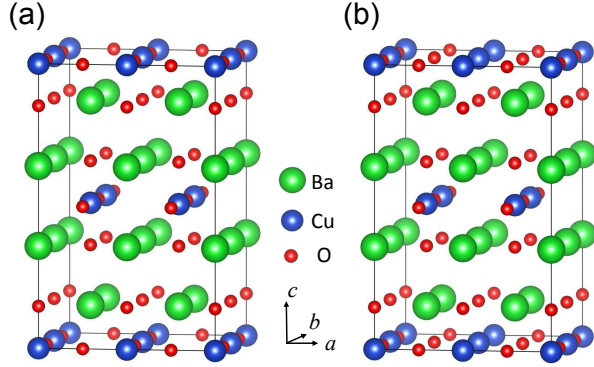


FIG. 6: Crystal structures with (a) the lowest energy state and (b) the second-lowest energy state for $\text{Ba}_2\text{CuO}_{3.25}$. They correspond to the 64-1* and 64-1 structures in Table III, respectively.

bands. In Figs. 5(c) and 5(d), we show the Fermi surface contours when the Fermi level is 0.05 and 0.1 eV below the top of the valence bands in the AFM Néel state, respectively. Upon small hole doping, a hole pocket emerges around the M point. When more holes are doped into the system, the hole pockets merge together to form flat Fermi surface sheets in the k_a - k_c plane.

B. Electronic and magnetic structures of $\text{Ba}_2\text{CuO}_{3+\delta}$

In high- T_c cuprates, superconductivity emerges when charge carriers, either holes or electrons, are doped into the parent compounds. It is commonly believed that AFM spin fluctuations play a very important role in pairing electrons^{39–41}. One can dope holes to Ba_2CuO_3 either by introducing extra oxygen atoms or by substituting Ba atoms with alkali atoms^{42,43}. The superconducting material $\text{Ba}_2\text{CuO}_{3+\delta}$ ^{25,44–46} can be regarded as a compound either by introducing more oxygens to Ba_2CuO_3 or by removing oxygens from Ba_2CuO_4 .

To know the electronic and magnetic structures of this material, it is important to know accurately where the oxygen vacancies are located. We investigated this problem using both the virtual crystal approximation approach and the supercell approach in the framework of density functional theory.

In the virtual crystal approach, we considered three different kinds of distributions of oxygen vacancies: (1) the vacancies are all located in the Cu-O layers, (2) the vacancies are all located in the Ba-O layers, and (3) the vacancies are equally partitioned in both kinds of layers. For a nominal component $\text{Ba}_2\text{CuO}_{3.2}$, the relative energies of the second and third cases with respect to the first case are found to be +1.88, and +92.58 eV/cell, respectively. This suggests that the oxygen vacancies prefer to reside in the Cu-O layers.

In the supercell approach, we calculated the energies for 26 possible structures of $\text{Ba}_2\text{CuO}_{3.25}$ (Figs. 6 and

TABLE II: Relative energies (in unit of meV/Cu) of the AFM1 state, the AFM dimer state, and the FM state with respect to that of the nonmagnetic state for Ba_2CuO_3 under different electron (e) and hole (h) doping concentrations (per Cu atom).

doping	AFM1	dimer	FM
0	-180	-116	-22
0.1 e	-97	-70	-35
0.15 e	-61	-58	-47
0.15 h	-79	-36	+11
0.3 h	-27	-13	-3

7) in a $2 \times 2 \times 1$ supercell with 6 oxygen vacancies. By comparison, we find that the two configurations shown in Figs. 6(a) and 6(b) have the lowest and the second lowest energies, respectively. In both cases, we also find that the Ba-O layer keeps intact, while the oxygen vacancies also prefer to locate in the Cu-O layers rather than occupying the apical oxygen positions. The relative total energies of these 26 structures are listed in Table III.

The results obtained from both approaches indicate that the oxygen vacancies are located in the Cu-O layers rather than in the Ba-O layers. This is consistent with the experimental data of neutron powder diffraction²⁶ and electron diffraction²⁷ measurements for $\text{Sr}_2\text{CuO}_{3+\delta}$.

To see how the magnetic order is changed by the doping in $\text{Ba}_2\text{CuO}_{3+\delta}$, we evaluated the energies of several different kinds of magnetic states. Since the inter-chain coupling is very weak, we ignore the difference of different magnetic ordered states along the a -axis and assume that the inter-chain coupling along the a -axis is ferromagnetic. Table II shows how the energies of four typical magnetic states (i.e. nonmagnetic, AFM1, AFM dimer, and FM states) vary with the electron or hole doping. As expected, the energy difference between the lowest-energy (AFM1) state and the second-lowest-energy (dimer) state is reduced with increasing doping. This suggests that the doping tends to induce magnetic frustrations⁴⁷ and enhance spin fluctuations, favoring the formation of superconducting Cooper pairs.

The above discussion suggests that it is Ba_2CuO_3 rather than Ba_2CuO_4 that is the parent compound of superconducting $\text{Ba}_2\text{CuO}_{3+\delta}$ materials^{25,44–46}. This can be more clearly seen by comparison with the other parent compounds of cuprate superconductors, such as La_2CuO_4 . First, like La_2CuO_4 , Ba_2CuO_3 is an AFM insulator. Second, Cu ions in Ba_2CuO_3 have the same +2 nominal valences as in La_2CuO_4 . Third, the highest occupied and the lowest unoccupied states in both compounds derive from the strongly hybridized O $2p$ orbitals and Cu $3d_{x^2-y^2}$ orbitals (for Ba_2CuO_3 , the bc plane is defined as the xy plane and $d_{x^2-y^2}$ is just the $d_{b^2-c^2}$ orbital).

TABLE III: Relative total energies (in unit of eV) for all 26 structures of $\text{Ba}_2\text{CuO}_{3.25}$ shown in Figs. 6 and 7 with oxygen vacancies in a $2 \times 2 \times 1$ supercell which contains 16 Ba atoms, 8 Cu atoms, 26 O atoms, and 6 O vacancies.

	BaO-1	BaO-2	82-1	82-2	82-3	73-1	73-2	64-1	64-2	64-3	64-4	64-5	64-6
ΔE	-1.871	0	-5.168	-4.450	-4.480	-6.350	-6.190	-8.173	-7.319	-7.069	-7.614	-7.380	-7.142
	55-1	55-2	55-3	55-4	64-1*	64-3*	64-4*	64-5*	64-6*	55-1*	55-2*	55-3*	55-4*
ΔE	-7.779	-7.736	-7.779	-7.711	-8.201	-7.042	-7.606	-7.401	-7.206	-7.729	-7.657	-7.704	-7.683

III. SUMMARY

We have studied the electronic and magnetic structures of $\text{Ba}_2\text{CuO}_{3+\delta}$ with δ varying from 0 to 1 by first-principles density functional theory calculations. Unlike Ba_2CuO_4 whose ground state is a non-magnetic metal, the ground state of Ba_2CuO_3 is found to be a quasi-one-dimensional AFM Mott insulator. The lowest unoccupied and highest occupied states in Ba_2CuO_3 are mainly contributed by Cu $3d_{b^2-c^2}$ orbitals and O $2p$ orbitals, respectively. By comparison of the total energies of $\text{Ba}_2\text{CuO}_{3+\delta}$ with different kinds of oxygen vacancy structures, we find that the oxygen vacancies reside mainly in the Cu-O layers (planar sites) rather than in the Ba-O layers (apical sites), in agreement with the experimental observation. Furthermore, doping of charge carriers to Ba_2CuO_3 can reduce the energy differences be-

tween different low-energy magnetic states and thus enhance the spin fluctuations. This suggests that Ba_2CuO_3 is the parent compound of oxygen doped $\text{Ba}_2\text{CuO}_{3+\delta}$ superconductors, and the AFM fluctuations in CuO chains play an important role in the superconducting pairing of electrons in these materials.

Acknowledgments

We thank C. Q. Jin for stimulating discussions. This work was supported by the National Key R&D Program of China (Grant No. 2017YFA0302900) and the National Natural Science Foundation of China (Grants No. 11774422 and No. 11774424). Computational resources were provided by the Physical Laboratory of High Performance Computing at Renmin University of China.

* Electronic address: kliu@ruc.edu.cn

† Electronic address: zlu@ruc.edu.cn

‡ Electronic address: txiang@iphy.ac.cn

¹ J. G. Bednorz and K. A. Müller, Z. Phys. B **64**, 189 (1986).

² G. R. Stewart, Adv. Phys. **66**, 75 (2017).

³ A. Schilling, M. Cantoni, J. D. Guo, and H. R. Ott, Nature **363**, 56 (1993).

⁴ L. Gao, Y. Y. Xue, F. Chen, Q. Xiong, R. L. Meng, D. Ramirez, C. W. Chu, J. H. Eggert, and H. K. Mao, Phys. Rev. B **50**, 4260(R) (1994).

⁵ E. Dagotto, Rev. Mod. Phys. **66**, 763 (1994).

⁶ A. J. Leggett, Nat. Phys. **2**, 134 (2006).

⁷ Y. Kamihara, T. Watanabe, M. Hirano, and H. Hosono, J. Am. Chem. Soc. **130**, 3296 (2008); X. H. Chen, T. Wu, G. Wu, R. H. Liu, H. Chen, D. F. Fang, Nature **453**, 761 (2008); G. F. Chen, Z. Li, D. Wu, G. Li, W. Z. Hu, J. Dong, P. Zheng, J. L. Luo, and N. L. Wang, Phys. Rev. Lett. **100**, 247002 (2008).

⁸ M. Rotter, M. Tegel and D. Johrendt, Phys. Rev. Lett. **101**, 107006 (2008).

⁹ X. C. Wang, Q. Q. Liu, Y. X. Lv, W. B. Gao, L. X. Yang, R. C. Yu, F. Y. Li, and C. Q. Jin, Solid State Commun. **148**, 538 (2008).

¹⁰ F. C. Hsu, J. Y. Luo, K. W. Yeh, T. K. Chen, T. W. Huang, P. M. Wu, Y. C. Lee, Y. L. Huang, Y. Y. Chu, D. C. Yan and M. K. Wu, Proc. Natl. Acad. Sci. U.S.A. **105**, 14262 (2008).

¹¹ X. F. Lu, N. Z. Wang, G. H. Zhang, X. G. Luo, Z. M.

Ma, B. Lei, F. Q. Huang, and X. H. Chen, Phys. Rev. B **89**, 020507 (2014); X. Dong, K. Jin, D. Yuan, H. Zhou, J.

Yuan, Y. Huang, W. Hua, J. Sun, P. Zheng, W. Hu, Y. Mao, M. Ma, G. Zhang, F. Zhou, and Z. Zhao, Phys. Rev. B **92**, 064515 (2015).

¹² D. Jérôme, A. Mazaud, M. Ribault, and K. Bechgaard, J. Phys. Lett. **41**, 95 (1980).

¹³ K. Bechgaard, K. Carneiro, M. Olsen, F. B. Rasmussen, and C. S. Jacobsen, Phys. Rev. Lett. **46**, 852 (1981).

¹⁴ J. C. Armici, M. Decroux, Φ. Fischer, M. Potel, R. Chevrel, and M. Sergent, Solid State Commun. **33**, 607 (1980).

¹⁵ M. Potel, R. Chevrel, and M. Sergent, J. Solid State Chem. **35**, 286 (1980).

¹⁶ Q.-G. Mu, B.-B. Ruan, K. Zhao, B.-J. Pan, T. Liu, L. Shan, G.-F. Chen, and Z.-A. Ren, Sci. Bull. **63**, 952 (2018).

¹⁷ J. K. Bao, J. Y. Liu, C. W. Ma, Z. H. Meng, Z. T. Tang, Y. L. Sun, H. F. Zhai, H. Jiang, H. Bai, C. M. Feng, Z. A. Xu, and G. H. Cao, Phys. Rev. X **5**, 011013 (2015).

¹⁸ Z. T. Tang, J. K. Bao, Y. Liu, Y. L. Sun, A. Ablimit, H. F. Zhai, H. Jiang, C. M. Feng, Z. A. Xu, and G. H. Cao, Phys. Rev. B **91**, 020506 (2015).

¹⁹ Z. T. Tang, J. K. Bao, Z. Wang, H. Bai, H. Jiang, Y. Liu, H. F. Zhai, C. M. Feng, Z. A. Xu, and G. H. Cao, Sci. China Mater. **58**, 16 (2015).

²⁰ Q. G. Mu, B. B. Ruan, B. J. Pan, T. Liu, J. Yu, K. Zhao, G. F. Chen, and Z. A. Ren, Phys. Rev. Mater. **2**, 034803 (2018).

²¹ Q. G. Mu, B. B. Ruan, B. J. Pan, T. Liu, J. Yu, K. Zhao, G.

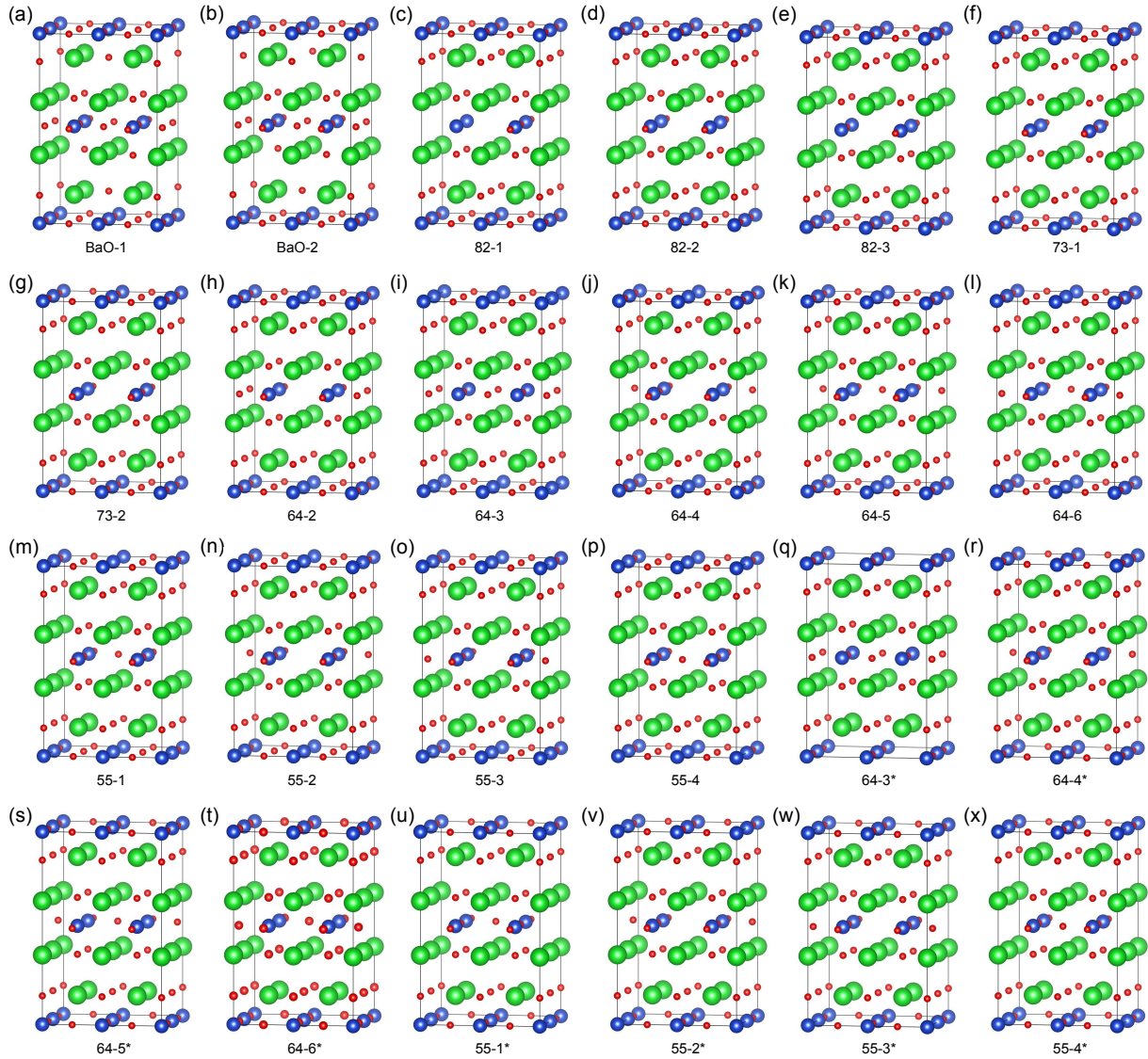


FIG. 7: Twenty-four possible structures of $\text{Ba}_2\text{CuO}_{3.25}$. For BaO-1 and BaO-2 structures, O vacancies are in the Ba-O layers. For mn - i structures, there are m and n O atoms in the bottom and middle Cu-O layers of the supercell, respectively. The green, blue, and red balls represent the Ba, Cu, and O atoms, respectively.

- F. Chen, and Z. A. Ren, Phys. Rev. B **96**, 140504 (2017).
- ²² T. Liu, Q. G. Mu, B. J. Pan, J. Yu, B. B. Ruan, K. Zhao, G. F. Chen, and Z. A. Ren, Europhys. Lett. **120**, 27006 (2017).
- ²³ Y. P. Qi, W. J. Shi, P. Werner, P. G. Naumov, W. Schnelle, L. Wang, K. G. Rana, S. Parkin, S. A. Medvedev, B. H. Yan, and C. Felser, npj Quantum Mater. **3**, 4 (2018).
- ²⁴ W. L. Wang, Y. M. Zhang, Y. F. Lv, H. Ding, L. L. Wang, W. Li, K. He, C. L. Song, X. C. Ma, and Q. K. Xue, Phys. Rev. B **97**, 134524 (2018).
- ²⁵ W. M. Li, L. P. Cao, J. F. Zhao, R. Z. Yu, J. Zhang, Y. Liu, Q. Q. Liu, G. Q. Zhao, X. C. Wang, Z. Hu, Q. Z. Huang, H. Wu, H. J. Lin, C. T. Chen, Z. Li, Z. Z. Gong, Z. Guguchia, J. S. Kim, G. Stewart, Y. W. Long, Y. J. Uemura, S. Uchida, and C. Q. Jin, arXiv:1808.09425.
- ²⁶ Y. Shimakawa, J. D. Jorgensen, J. F. Mitchell, B. A. Hunter, H. Shaked, D. G. Hinks, R. L. Hitterman, Z. Hiroi, and M. Takano, Physica C **228**, 73 (1994).
- ²⁷ H. Zhang, Y. Y. Wang, L. D. Marks, W. P. Dravid, P. D. Han, and D. A. Payne, Physica C **255**, 257 (1995).
- ²⁸ P. E. Blöchl, Phys. Rev. B **50**, 17953 (1994); G. Kresse and D. Joubert, Phys. Rev. B **59**, 1758 (1999).
- ²⁹ G. Kresse and J. Hafner, Phys. Rev. B **47**, 558 (1993); J. Phys.: Condens. Matter **6**, 8245 (1994).
- ³⁰ G. Kresse and J. Furthmüller, Comput. Mater. Sci. **6**, 15 (1996); Phys. Rev. B **54**, 11169 (1996).
- ³¹ J. P. Perdew, K. Burke, and M. Ernzerhof, Phys. Rev. Lett. **77**, 3865 (1996).
- ³² S. L. Dudarev, G. A. Botton, S. Y. Savrasov, C. J. Humphreys, and A. P. Sutton, Phys. Rev. B **57**, 1505 (1998).
- ³³ H.-Y. Cao, S.-Y. Chen, H.-J. Xiang, and X.-G. Gong, Phys.

- Rev. B **91**, 020504(R) (2015).
- ³⁴ K. Liu, Z.-Y. Lu, and T. Xiang, Phys. Rev. B **93**, 205154 (2016).
- ³⁵ H. Rosner, H. Eschrig, R. Hayn, S.-L. Drechsler, and J. Málek, Phys. Rev. B **56**, 3402 (1997).
- ³⁶ C. de Graaf and F. Illas, Phys. Rev. B **63**, 014404 (2000).
- ³⁷ K. Maiti, D. D. Sarma, T. Mizokawa, and A. Fujimori, Phys. Rev. B **57**, 1572 (1998).
- ³⁸ J. Schlappa, K. Wohlfeld, K. J. Zhou, M. Mourigal, M. W. Haverkort, V. N. Strocov, L. Hozoi, C. Monney, S. Nishimoto, S. Singh, A. Revcolevschi, J. Caux, L. Patthey, H. M. Rønnow, J. van den Brink, and T. Schmitt, Nature **485**, 82 (2012).
- ³⁹ P. A. Lee, N. Nagaosa, and X.-G. Wen, Rev. Mod. Phys. **78**, 17 (2006).
- ⁴⁰ T. Moriya and K. Ueda, Adv. Phys. **49**, 555 (2000).
- ⁴¹ D. J. Scalapino, Rev. Mod. Phys. **84**, 1383 (2012).
- ⁴² K. Ueno, S. Nakamura, H. Shimotani, A. Ohtomo, N. Kimura, T. Nojima, H. Aoki, Y. Iwasa, and M. Kawasaki, Nat. Mater. **7**, 855 (2008).
- ⁴³ A. T. Bollinger, G. Dubuis, J. Yoon, D. Pavuna, J. Misewich, and I. Božović, Nature **472**, 458 (2011).
- ⁴⁴ H. Yamamoto, M. Naito, and H. Sato, Jpn. J. Appl. Phys. **36**, L341 (1997).
- ⁴⁵ H. Yamamoto, M. Naito, and H. Sato, Physica C **338**, 29 (2000).
- ⁴⁶ S. Karimoto, H. Yamamoto, H. Sato, A. Tsukada, and M. Naito, J. Low Temp. Phys. **131**, 619 (2003).
- ⁴⁷ K. Liu, B.-J. Zhang, and Z.-Y. Lu, Phys. Rev. B **91**, 045107 (2015).